CHEMISTRY OF MATERIALS

Article

pubs.acs.org/cm

N-Doped Carbon-Wrapped Cobalt Nanoparticles on N-Doped Graphene Nanosheets for High-Efficiency Hydrogen Production

Weijia Zhou,*[,†] Jian Zhou,[‡] Yucheng Zhou,[†] Jia Lu,[†] Kai Zhou,[†] Linjing Yang,[†] Zhenghua Tang,[†] Ligui Li,[†] and Shaowei Chen*[,†,§]

[†]New Energy Research Institute, School of Environment and Energy, South China University of Technology, Guangzhou Higher Education Mega Center, Guangzhou, Guangdong 510006, China

[‡]National Laboratory of Solid State Microstructures and Department of Materials Science and Engineering, Nanjing University, Nanjing, Jiangsu 210093, China

[§]Department of Chemistry and Biochemistry, University of California, 1156 High Street, Santa Cruz, California 95064, United States

Supporting Information

ABSTRACT: Development of non-noble-metal catalysts for hydrogen evolution reaction (HER) with both excellent activity and robust stability has remained a key challenge in the past decades. Herein, for the first time, N-doped carbon-wrapped cobalt nanoparticles supported on N-doped graphene nanosheets were prepared by a facile solvothermal procedure and subsequent calcination at controlled temperatures. The electrocatalytic activity for HER was examined in 0.5 M H_2SO_4. Electrochemical measurements showed a small overpotential of only −49 mV with a Tafel slope of 79.3 mV/dec. Theoretical calculations based on density functional theory showed that the catalytically active sites were due to carbon atoms promoted by the entrapped cobalt nanoparticles. The results may offer a new methodology for the preparation of effective catalysts for water splitting technology.

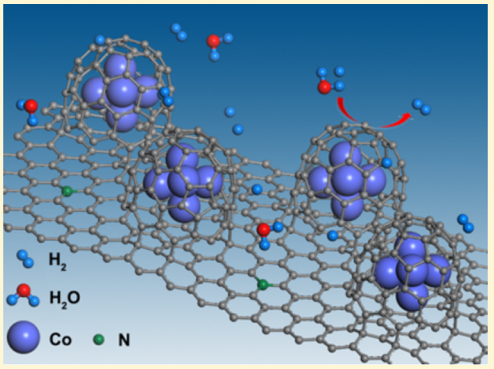

INTRODUCTION

With the ever increasing demand for energy and environmental protection on the global scale, development of technologies for clean and sustainable energy has been attracting increasingly intense attention. As an alternative and renewable energy source, hydrogen has been hailed as a promising candidate to ameliorate climate change and environmental problems associated with the combustion of fossil fuels. Hydrogen evolution reaction (HER) generates molecular hydrogen through the electrochemical reduction of water.[1−4] In these studies, advanced catalysts are essential to reduce the overpotential and increase the energy efficiency. To date, the most effective HER electrocatalysts are Pt-group metals, which exhibit a low overpotential to generate large cathodic current densities in highly acidic solutions.[5] However, the high costs and scarcity of these noble metals severely limit their broad utilization in energy systems. Therefore, it is of critical importance to develop highly active HER catalysts with a low overpotential based on earth-abundant and cost-effective materials, which has remained a great challenge thus far.

Toward this end, a variety of transition metal compounds, include MoS_2,[6,7] Mo_2C,[8] $CoSe_2$,[9] CoP,[10] and Ni_2P,[11] have been employed as effective non-Pt electrocatalysts for hydrogen production at low overpotentials.[12−14] Recently, Popczun et al.[10] reported that CoP nanoparticles with a diameter of ∼9 nm prepared by the decomposition of $[Co_2(CO)_8]$ in oil produced a cathodic current density of 20 mA/cm^2 at an overpotential of −95 mV. In addition, Zou et al.[15] reported the synthesis of cobalt embedded nitrogen-rich carbon nanotubes (CNTs), which were shown to be highly efficient electrocatalysts for HER in a wide range of pH, with a small onset potential of −50 mV and a low Tafel slope (69 mV/dec) in 0.5 M H_2SO_4. In these pioneering studies nonprecious transition metals (e.g., Co, Ni, etc.) were generally argued to be the active elements for HER electrocatalysis, a unique feature that significantly advances the design and engineering of HER electrocatalysts. However, the contributions from carbon are typically ignored, as carbon materials are primarily used as structural scaffolds for catalyst particles. In fact, studies have been scarce where water splitting is driven by carbon catalysts with a low overpotential.[16] Actually, the density of carbon electronic states may be modulated by transition metal elements such that carbon may also serve as active sites for HER.[17] This is the primary motivation of the present study.

Novel HER systems based on carbon-transition metals (Fe, Co, and Ni) were first reported by Asefa[15] and Bao[18,19] in 2014, which, however, were primarily confined to the fixed structure of catalysts (Fe, Co and Ni) encapsulated in carbon nanotubes. In the present study, N-doped carbon-wrapped Co nanoparticles with a size of about 15 nm supported on N-doped

Received: November 18, 2014
Revised: March 3, 2015
Published: March 5, 2015

DOI: 10.1021/acs.chemmater.5b00331
Chem. Mater. 2015, 27, 2026−2032

graphene nanosheets (Co@NC/NG) were synthesized by the decomposition of cyanamide and reduction of Co^{2+}, and characterized with a variety of experimental techniques. The influence of the core−shell structure of Co@NC/NG and valence state of Co on HER performance were also studied. Electrochemical studies showed that the obtained Co@NC/NG hybrids exhibited a remarkable electrocatalytic activity for HER, with the onset potential at only −49 mV (vs RHE) and excellent catalytic stability. The experimental results, in combination with theoretical calculations based on density functional theory (DFT), suggested that carbon served as the catalytically active sites and the activity was promoted by the entrapped cobalt nanoparticles.

EXPERIMENTAL METHODS

Materials. All reagents were of analytical grade and used without further purification. Cobalt acetate ($C_2H_3CoO_2$), cyanamide (DCDA, $C_2H_4N_4$), graphite powders, sulfuric acid (H_2SO_4), sodium nitrate ($NaNO_3$), and potassium permanganate ($KMnO_4$) and 20 wt % Pt/C were purchased from Sinopharm Chemical Reagents Beijing Co.

Synthesis of Graphene Oxide. Graphene oxide was prepared by acid oxidation of graphite powders according to the modified Hummers' method.[20] Briefly, graphite (3.0 g) was added to concentrated sulfuric acid (70 mL) under magnetic stirring at room temperature, into which sodium nitrate (1.5 g) was added, and then the mixture was cooled to 24 °C. Under vigorous agitation, potassium permanganate (9.0 g) was added slowly while the temperature of the solution was kept below 20 °C. The reaction mixture was then incubated in a 40 °C water bath for 30 min, forming a thick paste. Then, 140 mL of Nanopure water was added, and the solution was stirred for another 15 min. An additional 500 mL of water was added, followed by a slow addition of 20 mL of H_2O_2 (30%), and the color of the solution was found to turn from brown to yellow. The mixture was filtered and washed with a 1:10 HCl aqueous solution (250 mL) to remove metal ions, followed by repeated washing with water and centrifugation to remove excessive acid. The resulting solids were dispersed in water by sonication for 1 h at a concentration of 5 mg/mL.

Synthesis of N-Doped Carbon-Wrapped Co Nanoparticles on N-Doped Graphene Nanosheets (Co@NC/NG). The synthetic procedure is depicted in Figure 1, involving two major steps: (a) adsorption of Co^{2+} and cyanamide (DCDA) onto graphene oxide nanosheets; and (b) thermal decomposition of cyanamide and reduction of Co^{2+} to form N-doped carbon-wrapped Co nanoparticles on N-doped graphene nanosheets. In a typical reaction, 80 mg of cobalt acetate and 30 mg of cyanamide were codissolved in 20 mL of a water−ethanol solution (v:v = 1:1). The mixture was stirred at 80 °C for 1 h to form a cyanamide−Co complex. Afterward, 10 mL of a graphene oxide suspension (5 mg/mL) was added into the mixture and stirred for 1 h. Subsequently, the mixture was dried at 120 °C. The dried samples were placed into a covered crucible in a tube furnace, which were heated at 450 °C for 2 h, then at another controlled temperature (600 °C, 700 °C, 800 °C, or 900 °C) for 2 h under a N_2 atmosphere. The black products (denoted as Co@NC/NG) were then washed with a 1 M HCl aqueous solution to remove unwrapped Co particles.

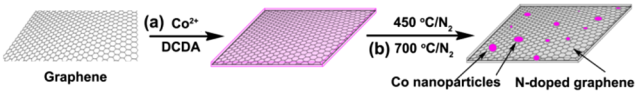

Figure 1. Schematic illustration of the synthesis of carbon-wrapped Co nanoparticles on N-doped graphene nanosheets (Co@NC/NG). (a) Adsorption of Co^{2+} and cyanamide (DCDA) onto graphene oxide nanosheets; (b) decomposition of cyanamide and reduction of Co^{2+} to form N-doped carbon-wrapped Co nanoparticles on N-doped graphene nanosheets.

Two control samples were prepared by using the same procedure but without the addition of cobalt acetate or cyanamide, which were donated as NC/NG and Co/G, respectively. A Co_3O_4/G sample was also prepared, where 60 mg cobalt acetate was added to 30 mL of a GO ethanol/water (v/v = 1:1) suspension and the reaction mixture was transferred to a 40 mL autoclave for hydrothermal reaction at 150 °C for 4 h.

Characterization. Field-emission scanning electron microscopic (FESEM, NOVA NanoSEM 430, FEI) measurements were employed to characterize the morphologies of the as-prepared samples. Transmission electron microscopic (TEM) measurements were carried out with a JEOL JEM 2100F microscope. Powder X-ray diffraction (XRD) patterns of the samples were recorded on a Bruke D8 Advance powder X-ray diffractometer with Cu Kα (λ = 0.15406 nm) radiation. X-ray photoelectron spectroscopic (XPS) measurements were performed using an ESCALAB 250. Raman spectra were acquired on a RENISHAW inVia instrument with an Ar laser source of 488 nm in a macroscopic configuration. The BET surface area was determined by Micromeritics ASAP 2010 with nitrogen adsorption at 77 K and the Barrett−Joyner−Halenda (BJH) method.

Electrochemistry. Electrochemical measurements were performed with an electrochemical workstation (CHI 760C, CH Instruments Inc.) in a 0.5 M H_2SO_4 aqueous solution. A Ag/AgCl electrode (saturated KCl) and a platinum wire were used as the reference and counter electrode, respectively. Four mg of the catalyst powders was dispersed in 1 mL of a 4:1 (v:v) water/ethanol mixed solvents along with 80 μL of a Nafion solution, and the mixture was sonicated for 30 min. Then, 5 μL of the above solution was dropcast onto the surface of a glassy carbon (GC) disk electrode at a catalyst loading of 0.285 mg/cm^2. The as-prepared catalyst film was dried at room temperature. Polarization curves were acquired by sweeping the potential from 0 to −0.8 V (vs Ag/AgCl) at a potential sweep rate of 5 mV/s. Accelerated stability tests were performed in 0.5 M H_2SO_4 at room temperature by potential cycling between 0 and −0.6 V (vs Ag/AgCl) at a sweep rate of 100 mV/s for a given number of cycles. Current−time responses were monitored by chronoamperometric measurements for 12 h.

In all measurements, the Ag/AgCl reference electrode was calibrated with respect to a reversible hydrogen electrode (RHE). The calibration was performed in a high-purity H_2 (99.999%) saturated electrolyte with a Pt wire as both the working electrode and counter electrode. Cyclic voltammograms (CVs) were collected at a scan rate of 1 mV/s, and the average of the two potentials at which the current crossed zero was taken as the thermodynamic potential for the hydrogen electrode reactions. In 0.5 M H_2SO_4, E(Ag/AgCl) = E(RHE) + 0.273 V.

Theoretical Calculations. The geometric and electronic properties of Co@NC/NG were calculated by density functional theory studies in the generalized gradient approximation implemented in the Vienna Ab initio Simulation Package (VASP), in which the projected augmented wave method and Perdew−Burke−Ernzerhof exchange correlation were used. The plane-wave cutoff energy was 520 eV throughout the calculations. The Brillouin zone integrations were performed with a Γ-center k-point mesh and the Gaussian smearing width was 0.05 eV. In order to simulate the carbon-wrapped Co nanoparticles (Co@C), we constructed Co atoms in a carbon cage. Then the atomic positions were relaxed by using the conjugate-gradient algorithm until the residual forces of all atoms were less than 0.02 eV/Å.

RESULTS AND DISCUSSION

The morphologies of the as-prepared Co@NC/NG were first examined by FESEM and (HR)TEM measurements, which are shown in Figure 2. From panel a, it can be seen that the Co@NC/NG hybrids exhibited a wrinkled surface; and refolding might also occur by the graphene sheets, as depicted in panel b. XRD measurements in panel c showed a broad peak at 25.5°, corresponding to the graphene (002) crystal planes, and an

DOI: 10.1021/acs.chemmater.5b00331
Chem. Mater. 2015, 27, 2026−2032

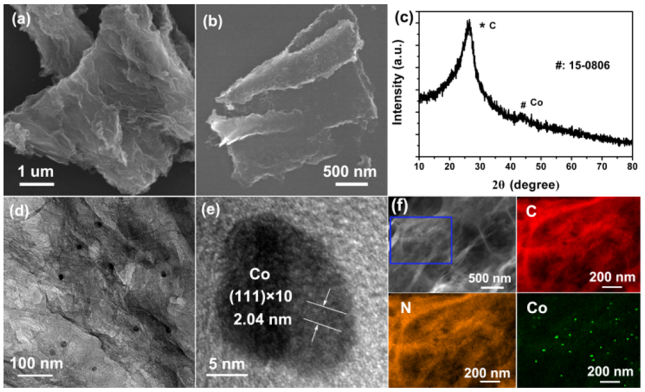

Figure 2. Representative (a, b) SEM images, (c) XRD, and (d, e) TEM images of Co@NC/NG (700 °C). (f) EDS elemental maps of C, N, and Co for Co@NC/NG (700 °C).

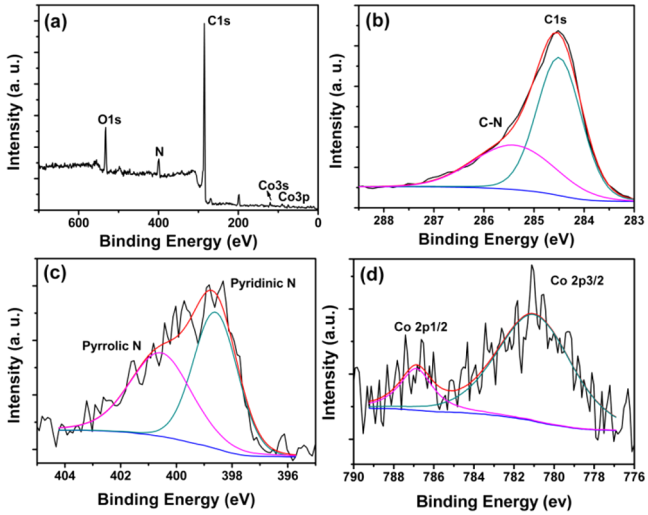

Figure 3. (a) XPS survey spectra and high-resolution scans of (b) C 1s, (c) N 1s, and (d) Co 2p electrons of Co@NC/NG (700 °C).

additional weak one at ca. 44.2°, which is consistent with the (111) crystal planes of cobalt (JCPDS No.15−0806, cubic, $a = b = c = 0.354$ nm), indicating the successful production of Co/C composites. Raman spectroscopic studies further confirmed that the formation of Co nanoparticles with a pair of characteristic peaks at 467.8 and 668.5 cm^{-1},[21] along with the D and G bands at 1326.5 and 1587.2 cm^{-1} for graphene (Figure S1 in the Supporting Information). Note that prior to HCl washing, a large number of Co nanoparticles (diameters of a few tens of nanometers) could be clearly seen on the surface of the graphane nanosheets with much more intense diffraction peaks for cobalt (Figure S2 in the Supporting Information).

Figure 2d, e show two representative TEM images of the resulting Co@NC/NG hybrids. It can be seen that the surface of the graphene nanosheets (dark gray background) were decorated with some dark-contrast objects that were most likely Co nanoparticles. It is worth noting that porous carbon film decomposed from cyanamide was covered on the surface of graphene nanosheets (Figure S3 in the Supporting Information). From Figure 2e, the Co(111) crystal planes can be clearly seen with a lattice spacing of 0.204 nm, with the particle diameters of 15−20 nm. Furthermore, elemental mapping based on energy dispersive X-ray (EDS) analysis (element contents were shown in Figure S4 in the Supporting Information) clearly shows that the Co@NC/NG hybrids consists of C, N, Co, and O (not shown) elements (Figure 2f), and nitrogen was evenly distributed with the C element, implying that N element was indeed doped into the porous carbon film and graphene nanosheets, whereas Co was found discretely, which is consistent with the TEM micrograph in panel d.

XPS measurements were then carried out to determine the elemental compositions and valence states of the Co@NC/NG hybrids. As depicted in Figure 3a, only the elements of carbon, nitrogen, oxygen, and cobalt can be easily identified. Deconvolution of the high-resolution scan of the N 1s electrons yielded two peaks at 398.5 and 400.5 eV (Figure 3c), which were consistent with pyridinic and pyrollic nitrogen, respectively, indicating the successful incorporation of N into the porous carbon and graphene matrix.[22] The N doping was also observed in the survey spectrum for C 1s electrons in Figure 3b, which shows a peak at 285.4 eV characteristic of carbon in C−N. For the Co 2p electrons (Figure 3d), a doublet can be identified at 787.1 and 781.1 eV. These are 3−4 eV higher than those of bulk cobalt.[23,24] Note that in XRD and TEM measurements (Figures 2 and Figure S2 in the Supporting Information), only metallic Co was identified in the Co@NC/NG sample. Thus, the substantial blue shifts of the binding energy of the Co 2p electrons in Co@NC/NG suggest that electron transfer occurred from Co to C (vide infra). Furthermore, on the basis of the integrated peak areas, the atomic contents of Co and N in Co@NC/NG were estimated to be 0.48 and 7.5 at %, respectively.

The electrocatalytic activities of Co@NC/NG for HER were then examined by electrochemical measurements in 0.5 M H_2SO_4. From Figure 4a, apparent nonzero cathodic currents can be seen at the electrode modified by Co@NC/NG (magenta curve) with an onset potential of −0.049 V (vs RHE), which is markedly better than those of NC/NG (−0.337 V, black curve), Co_3O_4/G (−0.409 V, red curve; with XRD data depicted in Figure S5 in the Supporting Information), and Co/G (−0.331 V, blue curve; with XPS data shown in Figure S6 in the Supporting Information) at the same catalyst loading. Furthermore, it is important to note that when Co nanoparticles were loaded on the graphene surface but without the carbon coating layer (Co/NC/NG, green curve), the HER performance was markedly poorer than that of Co@NC/NG (onset potential −0.172 V), despite similar chemical compositions. These results indicate that both N-doped carbon coating and valence state of cobalt played an important role in enhancing the HER activity, although the overall activity remains subpar as compared to that of commercial 20 wt % Pt/C catalysts (onset potential −0.008 V, yellow/green curve).

The linear portions of the Tafel plots were fitted to the Tafel equation ($\eta = b\log j + a$, where j is the current density and b is the Tafel slope), yielding Tafel slopes of 79.3 mV/dec and 31.6 mV/dec for Co@NC/NG and 20 wt % Pt/C, respectively (Figure 4b), which are markedly lower than those of NC/NG (182.5 mV/dec), Co_3O_4/G (186.8 mV/dec), Co/G (143.6 mV/dec), and Co/NC/NG (111.2 mV/dec). Note that for hydrogen evolution in acid solutions on metal electrode surfaces, the mechanism typically involves three major reactions.[7,12,25]

DOI: 10.1021/acs.chemmater.5b00331
Chem. Mater. 2015, 27, 2026−2032

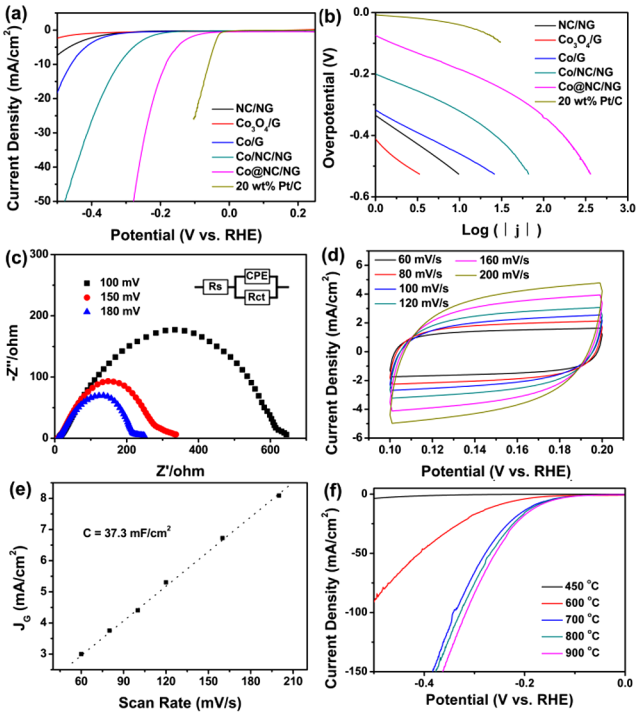

Figure 4. (a) Polarization curves for HER in 0.5 M H_2SO_4 at a glassy carbon electrode modified with NC/NG, Co_3O_4/G, Co/G, Co/NC/NG, Co@NC/NG (700 °C), and 20 wt % Pt/C, respectively. Potential sweep rate 5 mV/s. (b) Corresponding Tafel plots derived from a. (c) Nyquist plots and the equivalent circuit of the Co@NC/NG (700 °C)-modified electrode at various HER overpotentials in 0.5 M H_2SO_4. (d) Cyclic voltammograms within the range of +0.1 to +0.2 V where no faradaic reactions occurred. (e) Variation of double-layer charging currents at +0.15 V with potential scan rate. Symbols are experimental data acquired from panel (d), and dotted line is linear regression. (f) Polarization curves for Co@NC/NG prepared at different annealing temperatures (450, 600, 700, 800, and 900 °C).

$$H_3O^+ + \text{e-catalyst} \leftrightarrow \text{H-catalyst} + H_2O \text{ (Volmer reaction, Tafel slope 120 mV/dec)} \quad (1)$$

$$2\text{H-catalyst} \leftrightarrow H_2\text{-catalyst (Tafel reaction, Tafel slope 30 mV/dec)} \quad (2)$$

$$H_3O^+ + \text{e-catalyst} + \text{H-catalyst} \leftrightarrow H_2\text{-catalyst} + \text{catalyst} + H_2O \text{ (Heyrovsky reaction, Tafel slope 40 mV/dec)} \quad (3)$$

where e-catalyst denotes metal-bound electrons, and H-catalyst and H_2-catalyst represent a hydrogen atom and a hydrogen molecule adsorbed on to a surface metal atom, respectively. These reactions are dependent on the inherent (electro)-chemical and electronic properties of the catalyst surface. Experimentally two main pathways are generally observed for HER, Volmer–Tafel reaction (eqs 1 and 2) and Volmer–Heyrovsky reaction (eqs 1 and 3). In the present study, the Tafel slope of 79.3 mV/dec for Co@NC/NG suggests that HER was likely controlled by both the first-electron reduction of protons and electrochemical desorption of hydrogen (Volmer–Heyrovsky reaction).

Electrochemical impedance spectroscopy (EIS) is also a powerful technique in the characterization of interfacial reactions and electrode kinetics in HER. Figure 4c showed the representative Nyquist plots of the Co@NC/NG-modified electrode at various overpotentials. More detailed analyses were carried out by fitting the impedance data to an equivalent circuit, where a constant phase element (CPE) was employed, as depicted in the inset to panel c. The solution resistance (R_s) was estimated to be about 14.2 Ω, and the charge transfer resistance (R_{ct}) was found to decrease significantly with increasing overpotentials, from 492.2 Ω at −100 mV to 171.3 Ω at −180 mV. The lower resistance suggests a faster HER at higher overpotentials.

With regards to current density the performance of Co@NC/NG is also remarkable. Note that voltammetric study within the potential range of +0.1 to +0.2 V, where no faradaic reaction occurred (Figure 4d, e), showed that the double-layer capacitance of the Co@NC/NG (loading 0.285 mg/cm^2) modified electrode was 37.3 mF/cm^2, markedly higher than or comparable with literature results, such as $CoSe_2$ nanoparticles/carbon fiber paper (14.1 mF/cm^2, loading: 3.0 mg/cm^2)[9] and metallic WS_2 nanosheets (47.8 mF/cm^2, loading: 1.0 mg/cm^2).[26] This suggests a large effective electrochemical surface area of the mesoporous carbon coated graphene nanosheets. Consistent results were obtained in nitrogen adsorption/desorption studies (Figure S7 in the Supporting Information), where the specific surface area was estimated to be 217.4 m^2/g with a hierarchical porous structure, which almost doubled that of pure graphene nanosheets (127.3 m^2/g, Figure S8 in the Supporting Information).

The effects of carbonization temperature on the morphologies and structure of Co@NC/NG were then probed by SEM and Raman measurements. From Figure 5, it can be seen that similar nanosheets were produced at annealing temperatures ranging from 600 to 900 °C (Figures 2a and 5a–c). As the temperature increased from 600 to 900 °C, the I_D/I_G (graphene

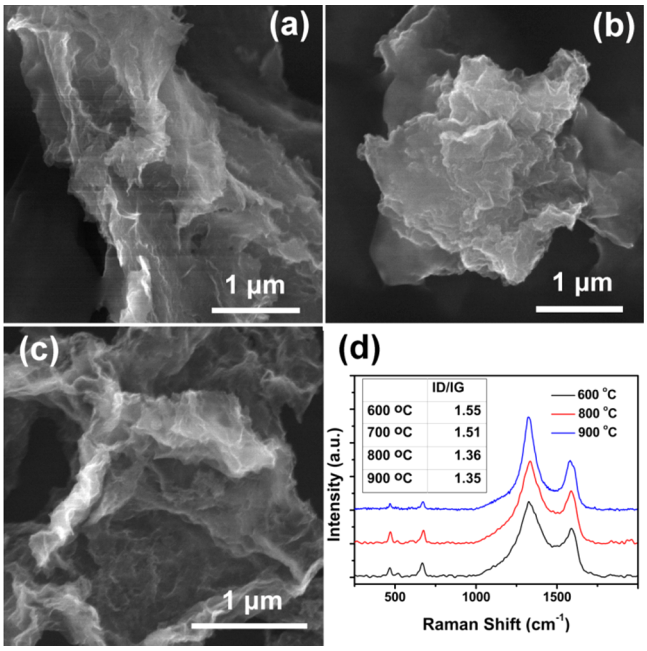

Figure 5. (a–c) SEM images and (d) Raman spectra of Co@NC/NG prepared at different annealing temperatures: (a) 600, (b) 800, and (c) 900 °C.

DOI: 10.1021/acs.chemmater.5b00331
Chem. Mater. 2015, 27, 2026–2032

D and G bands) ratios of Co@NC/NG decreased from 1.55 to 1.35, indicating an increasing degree of graphitization (Figure 5d). The corresponding HER performance was then examined by voltammetric measurements. As depicted in Figure 4f, the onset potential for HER was found to be rather similar (about −0.049 V) among the samples prepared at different calcination temperatures (600 to 900 °C). Yet, the cathodic current density exhibited a clear variation. For instance, at −0.30 V the cathodic current density increased in the order of 600 °C (−17.1 mA/cm^2) < 700 °C (−65.8 mA/cm^2) < 800 °C (−74.1 mA/cm^2) < 900 °C (−82.7 mA/cm^2). Taken together, these results suggest that 700−900 °C appeared to be the optimal range of calcination temperature in the preparation of Co@NC/NG for HER electrocatalysis.

In addition to good catalytic activity, the Co@NC/NG electrode also exhibited extraordinary stability for HER. Figure 6a shows that, even after 1000 potential cycles, the $j-V$ curve of

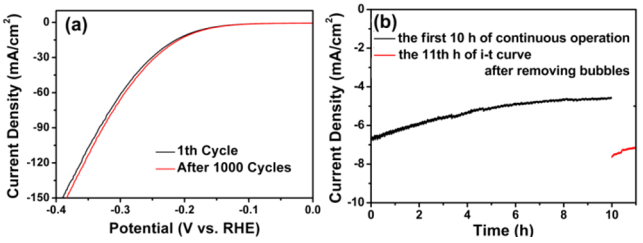

Figure 6. (a) HER polarization curves for Co@NC/NG (700 °C) before and after 1000 potential cycles in the stability test. (b) Current−time plots of the Co@NC/NG (700 °C) electrode at the applied potential of −0.223 V (vs RHE) before (black curve) and after (red curve) removing H_2 bubbles from the electrode surface.

the Co@NC/NG (700 °C) electrode remained almost unchanged, indicating long-term viability under operating conditions. The reverse scans also confirmed the robust HER stability of the Co@NC/NG (700 °C) electrode (Figure S9 in the Supporting Information). To further verify the stability of Co@NC/NG (700 °C) in HER, the current−time plots at the applied potential of −0.223 V (vs RHE) was depicted in Figure 6b. The current diminished by about 29.8% over 10 h of continuous operation, from −6.56 to −4.6 mA/cm^2. This is mainly because of H_2 bubbles gathered on the electrode surface. In fact, after H_2 bubbles were removed from the electrode surface, the current density returned to the original level, even with a small increase (−7.6 mA/cm^2, Figure 6b). Further tests of the catalytic durability of Co@NC/NG were conducted by loading the catalysts on carbon paper, where the current was found to remain almost unchanged for 5 h of continuous operation (Figure S10 in the Supporting Infomration). This further demonstrates the strong durability of the Co@NC/NG (700 °C) electrode for HER in 0.5 M H_2SO_4.

Notably, the HER performance of the obtained Co@NC/NG, within the context of onset potential (−49 mV vs RHE), current density (13.6 mA/cm^2 at −0.2 V), and Tafel slope (79.3 mV/dec), is markedly better than or comparable to those of Mo-based HER catalysts, such as MoS_2/reduced graphene (~100 mV, 48 mA/cm^2, 41 mV/dec),[7] nickel−molybdenum nitride nanosheets (~78 mV, 4 mA/cm^2, 35.9 mV/dec),[27] and Co-carbon based HER catalysts such as cobalt-embedded nitrogen-rich carbon nanotubes (~50 mV, 6 mA/cm^2, 80 mV/dec),[15] CoS_2 nanowire array (~145 mV at 10 mA/cm^2, 51.6 mV/dec),[26] C_3N_4@N-doped graphene (12 mV, 2.5 mA/cm^2, 51.5 mV/dec). These are also listed in Table S1 in the Supporting Information. One can see that Co-carbon based HER catalysts generally exhibit possess lower onset potentials, but higher Tafel slopes than Mo-based HER catalysts.

To unravel the fundamental mechanism responsible for this remarkable HER performance, we performed DFT calculations by using the Vienna Ab-initio Simulation Package (VASP) code.[28,29] The generalized gradient approximation with the Perdew−Burke−Ernzerhof exchange correlation[30] and projected augmented wave method[31,32] were used in the calculations, with a plane-wave cutoff energy of 520 eV. For simplicity, we have used a C_{60} molecule with a Co atom in it to simulate the carbon-wrapped Co nanoparticles in the experiments. A pure C_{60} molecule was also calculated for comparison.

The model entails a Co nanoparticle trapped inside a carbon cage (Co@C) (Figure 7a). Note that DFT calculations of N-

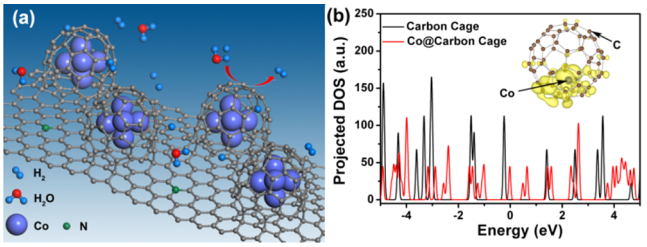

Figure 7. Results of DFT calculations: (a) Schematic representation of the HER process at the surface of Co@NC/NG, with gray C, red O, blue H, bluish violet Co, and green N atoms. (b) Electron density of states of a Co@C cage (red line) and a pure C cage (black line). The Fermi level is 0 eV. Inset in b shows the optimized structure and HOMO of the Co@C cage. The yellow regions indicate a charge increase.

doped graphene with decreased adsorption free energy have been reported in previous results.[15,33] To simplify the calculation program, we ignored the N-doping effect on the charge density of Co@NC/NG in the calculations. Figure 7b depicts the density of state (DOS) of the Co@C cage and pure C cage, which were broadened from the molecular energy level with a smearing factor of 0.05 eV. It can be seen that the HOMO−LUMO gap of the pure C cage was about 1.6 eV. When a Co atom was inserted into the C cage, it adsorbed on the top of the hollow sites of a carbon hexagon with a Co−C bond length of about 2.01 Å. About 0.7 electron was transferred from Co to the nearby carbon atoms by the bader charge anlaysis, raising the Fermi level. The Co atom also introduced some energy levels in the HOMO−LUMO gap of the pure C cage. It was found that the molecular orbital near the Fermi energy arose primarily from the Co and some nearby carbon atoms. One can see that the HOMO in Figure 7b was localized near the Co atom. This effect was further illustrated by the different charge−density distribution as shown in the inset to Figure 7b, in which an increase of the pz charge density can be clearly seen at the C atoms surrounding the Co atom. Note that electron transfer from Co to C atoms was suggested in XPS measurements (Figure 3). Charge transfer and the local molecule orbital near the Co were expected to decrease the local work function and increase chemical reactivity, leading to enhanced HER activity, as observed experimentally.

On the basis of the above results, in conjunction with recent studies of nitrogen-doped graphene and Co-based electrocatalysts, the following possible synergistic catalytic effects are

DOI: 10.1021/acs.chemmater.5b00331
Chem. Mater. 2015, 27, 2026−2032

proposed to account for the enhanced HER catalytic activity of Co@NC/NG. First, graphene nanosheets acted as an interconnected conducting network and afforded the selective growth of highly dispersed Co nanoparticles on graphene and enabled rapid electron transport from the Co nanoparticles to the electrodes via electronic coupling. Second, nitrogen atoms are inherently advantageous in interacting with H^+ than carbon atoms because of the presence of lone-pair electrons, which are known as favorable for both the interaction and reactivity.[15,33] Third, the Co nanoparticles were crucial for the HER, which not only decreased the local work function on the carbon surface, but also changed the electronic density of states around the carbon, resulting in the generation of additional catalytic active sites from carbon atoms, as confirmed in DFT calculations (Figure 7). Similar results have also been reported for oxygen reduction reaction (ORR)[34] and oxygen evolution reaction (OER).[35] The above speculation that catalytic active sites arose from carbon atoms was consistent with the core−shell structure of Co@C. The Co nanoparticles were not in contact with the electrolyte of 0.5 M H_2SO_4. Therefore, the Co@C core−shell structure not only ensured that the metals were not dissolved in acidic electrolyte (Figure S11 in the Supporting Information) but also enhanced the HER activity via the synergetic effect between Co and C.[18] In contrast, Co_3O_4/G and Co/G displayed poor HER activity, as shown in Figure 4a. Such a strategy of "metal induced catalytic activity of carbon" might be generalized in the synthesis and engineering of HER catalysts based on carbon and metal elements.

CONCLUSIONS

In this study, an efficient electrocatalyst based on earth-abundant and cost-effective components has been developed for hydrogen evolution reaction. N-doped carbon wrapped Co nanoparticles on N-doped graphene nanosheets (Co@NC/NG) were produced by decomposition of cyanamide and concurrent reduction of Co^{2+}. The N-doped carbon wrapped Co nanoparticles were loaded on the surface of N-doped graphene nanosheets, and the resulting composites were found to possess high electronic conductivity and abundant active sites for HER. Electrochemical studies showed that the catalysts exhibited excellent HER activity with an onset potential of −49 mV (vs RHE), a large current density, a small Tafel slope of 79.3 mV/dec, as well as prominent electrochemical durability. Theoretical studies based on DFT calculations showed that the catalytic active sites likely arose from carbon atoms, which were promoted by the entrapped Co nanoparticles. These combined results indicate that the synergetic interactions among the core−shell structure, N-doped treatment and valence state of cobalt play important roles in enhancing the HER activity of Co@NC/NG. Such a strategy of "metal induced catalytic activity of carbon" might be exploited as a novel effective paradigm for the design, engineering and optimization of composite HER catalysts based on carbon and metal elements.

ASSOCIATED CONTENT

Supporting Information

Additional discussion and Figures S1−S11. This material is available free of charge via the Internet at http://pubs.acs.org.

AUTHOR INFORMATION

Corresponding Authors

*E-mail: eszhouwj@scut.edu.cn.

*E-mail: shaowei@ucsc.edu.

Notes

The authors declare no competing financial interest.

ACKNOWLEDGMENTS

This work was supported by the National Recruitment Program of Global Experts, the PhD Start-up Funds of the Natural Science Foundation of Guangdong Province (S2013040016465), and Zhujiang New Stars of Science & Technology (2014J2200061).

REFERENCES

(1) Subbaraman, R.; Tripkovic, D.; Strmcnik, D.; Chang, K.-C.; Uchimura, M.; Paulikas, A. P.; Stamenkovic, V.; Markovic, N. M. *Science* **2011**, *334* (6060), 1256−1260.

(2) Zhou, W.; Wu, X.-J.; Cao, X.; Huang, X.; Tan, C.; Tian, J.; Liu, H.; Wang, J.; Zhang, H. *Energy Environ. Sci.* **2013**, *6* (10), 2921−2924.

(3) Yang, J.; Voiry, D.; Ahn, S. J.; Kang, D.; Kim, A. Y.; Chhowalla, M.; Shin, H. S. *Angew. Chem., Int. Ed.* **2013**, *52* (51), 13751−13754.

(4) Xie, J.; Zhang, H.; Li, S.; Wang, R.; Sun, X.; Zhou, M.; Zhou, J.; Lou, X. W.; Xie, Y. *Adv. Mater.* **2013**, *25* (40), 5807−5813.

(5) Stephens, I. E. L.; Chorkendorff, I. *Angew. Chem., Int. Ed.* **2011**, *50* (7), 1476−1477.

(6) Gopalakrishnan, D.; Damien, D.; Shaijumon, M. M. *ACS Nano* **2014**, *8* (5), 5297−5303.

(7) Li, Y.; Wang, H.; Xie, L.; Liang, Y.; Hong, G.; Dai, H. *J. Am. Chem. Soc.* **2011**, *133* (19), 7296−7299.

(8) Wan, C.; Regmi, Y. N.; Leonard, B. M. *Angew. Chem., Int. Ed.* **2014**, *53* (25), 6407−6410.

(9) Kong, D.; Wang, H.; Lu, Z.; Cui, Y. *J. Am. Chem. Soc.* **2014**, *136* (13), 4897−4900.

(10) Popczun, E. J.; Read, C. G.; Roske, C. W.; Lewis, N. S.; Schaak, R. E. *Angew. Chem., Int. Ed.* **2014**, *53* (21), 5427−5331.

(11) Popczun, E. J.; McKone, J. R.; Read, C. G.; Biacchi, A. J.; Wiltrout, A. M.; Lewis, N. S.; Schaak, R. E. *J. Am. Chem. Soc.* **2013**, *135* (25), 9267−9270.

(12) Zhou, W.; Hou, D.; Sang, Y.; Yao, S.; Zhou, J.; Li, G.; Li, L.; Liu, H.; Chen, S. *J. Mater. Chem. A* **2014**, *2* (29), 11358−11364.

(13) Chang, Y.-H.; Lin, C.-T.; Chen, T.-Y.; Hsu, C.-L.; Lee, Y.-H.; Zhang, W.; Wei, K.-H.; Li, L.-J. *Adv. Mater.* **2013**, *25* (5), 756−760.

(14) Xie, J.; Zhang, J.; Li, S.; Grote, F.; Zhang, X.; Zhang, H.; Wang, R.; Lei, Y.; Pan, B.; Xie, Y. *J. Am. Chem. Soc.* **2013**, *135* (47), 17881−17888.

(15) Zou, X.; Huang, X.; Goswami, A.; Silva, R.; Sathe, B. R.; Mikmeková, E.; Asefa, T. *Angew. Chem., Int. Ed.* **2014**, *53* (17), 4372−4376.

(16) Das, R. K.; Wang, Y.; Vasilyeva, S. V.; Donoghue, E.; Pucher, I.; Kamenov, G.; Cheng, H.-P.; Rinzler, A. G. *ACS Nano* **2014**, *8* (8), 8447−8456.

(17) Gong, K.; Du, F.; Xia, Z.; Durstock, M.; Dai, L. *Science* **2009**, *323* (5915), 760−764.

(18) Deng, J.; Ren, P.; Deng, D.; Yu, L.; Yang, F.; Bao, X. *Energy Environ. Sci.* **2014**, *7* (6), 1919−1923.

(19) Wang, J.; Gao, D.; Wang, G.; Miao, S.; Wu, H.; Li, J.; Bao, X. *J. Mater. Chem. A* **2014**, *2* (47), 20067−20074.

(20) Hummers, W. S.; Offeman, R. E. *J. Am. Chem. Soc.* **1958**, *80* (6), 1339−1339.

(21) Rakhi, R. B.; Chen, W.; Cha, D.; Alshareef, H. N. *Nano Lett.* **2012**, *12* (5), 2559−2567.

(22) Qu, L.; Liu, Y.; Baek, J.-B.; Dai, L. *ACS Nano* **2010**, *4* (3), 1321−1326.

(23) Biesinger, M. C.; Payne, B. P.; Grosvenor, A. P.; Lau, L. W. M.; Gerson, A. R.; Smart, R. S. C. *Appl. Surf. Sci.* **2011**, *257* (7), 2717−2730.

(24) Yan, J.-M.; Zhang, X.-B.; Shioyama, H.; Xu, Q. *J. Power Sources* **2010**, *195* (4), 1091−1094.

(25) Thomas, J. G. N. *Trans. Faraday Soc.* **1961**, *57* (0), 1603−1611.

(26) Faber, M. S.; Dziedzic, R.; Lukowski, M. A.; Kaiser, N. S.; Ding, Q.; Jin, S. *J. Am. Chem. Soc.* **2014**, *136* (28), 10053−10061.

DOI: 10.1021/acs.chemmater.5b00331
Chem. Mater. 2015, 27, 2026−2032

(27) Chen, W.-F.; Sasaki, K.; Ma, C.; Frenkel, A. I.; Marinkovic, N.; Muckerman, J. T.; Zhu, Y.; Adzic, R. R. *Angew. Chem., Int. Ed.* **2012**, *51* (25), 6131−6135.
(28) Kresse, G.; Hafner, J. *Phys. Rev. B* **1993**, *48* (17), 13115−13118.
(29) Kresse, G.; Furthmüller, J. *Comput. Mater. Sci.* **1996**, *6* (1), 15−50.
(30) Perdew, J. P.; Burke, K.; Ernzerhof, M. *Phys. Rev. Lett.* **1996**, *77* (18), 3865−3868.
(31) Blöchl, P. E. *Phys. Rev. B* **1994**, *50* (24), 17953−17979.
(32) Kresse, G.; Joubert, D. *Phys. Rev. B* **1999**, *59* (3), 1758−1775.
(33) Chen, S.; Duan, J.; Jaroniec, M.; Qiao, S.-Z. *Adv. Mater.* **2014**, *26* (18), 2925−2930.
(34) Deng, D.; Yu, L.; Chen, X.; Wang, G.; Jin, L.; Pan, X.; Deng, J.; Sun, G.; Bao, X. *Angew. Chem., Int. Ed.* **2013**, *52* (1), 371−375.
(35) Zhuang, Z.; Sheng, W.; Yan, Y. *Adv. Mater.* **2014**, *26* (23), 3950−3955.

DOI: 10.1021/acs.chemmater.5b00331
Chem. Mater. 2015, 27, 2026−2032